ARTICLES

On the Stacking Behavior of Functionalized Single-Wall Carbon Nanotubes

A. Kukovecz,*,† Ch. Kramberger,† M. Holzinger,‡ H. Kuzmany,† J. Schalko,§ M. Mannsberger,† and A. Hirsch‡

Institut für Materialphysik, Universität Wien, Strudlhofgasse 4., A-1090 Wien, Austria; Institut für Organische Chemie, Universität Erlangen, Henkestrasse 42, D-91054 Erlangen, Deutschland; and Fakultät für Elektrotechnik und Informationstechnik, TU Wien, Gusshausstrasse 27-29, A-1040 Wien, Austria

Received: October 31, 2001; In Final Form: March 4, 2002

Single-wall carbon nanotubes (SWNTs) were oxidatively functionalized by nitric acid treatment. The presence of carboxyl groups was proven by IR spectroscopy, matching earlier IR and NMR observations. Raman spectra in the radial breathing mode (RBM) and G line spectral windows were measured with six laser lines ranging from 457 to 647 nm. The RBM mode was observed to upshift by the functionalization with very little change in the spectral line shape. By the analysis of the spectral moments of the lines, this upshift is interpreted as a change in an empirical intertube interaction function. In agreement with previous TEM results, we have found that bundles in a pristine SWNT sample are significantly thinner (<10 tubes) than those in the oxidized samples (>30 tubes). Changes observed in solvatation properties and sample morphology could be explained on this basis. Our observations suggest that carboxyl related secondary bonding forces might also play a role in the stacking of oxidized SWNTs.

Introduction

Single-wall carbon nanotubes (SWNTs) have been in the focus of scientific attention ever since their discovery in 1993.[1] Most often visualized as rolled-up graphite sheets with diameters between 0.5 and 2 nm and lengths of several micrometers, these unique structures are expected to have a serious impact on nanoindustry soon. The two most widespread SWNT synthesis methods, dc arc discharge and laser ablation, are both able to supply nanotubes with rates up to several tens of grams per day in purities exceeding 70%. Very recently a mass production method producing up to 1.24 g/min 50% purity material was described by Ando et al.[2] Therefore, it is safe to assume that the present quantity demand for SWNTs can be sufficed. On the other hand, the development of real-life SWNT applications is seriously hindered by the poor reliability and control over the quality of the prepared material.

The properties of single-wall nanotubes are determined by the Hamada vector, the folding vector along which the graphite sheet is rolled up into itself. It is widely accepted to refer to SWNTs by the (*n, m*) indexes of this vector. The (*n, n*) or "armchair" tubes are always metallic, whereas the (*n*, 0) "zigzag" and (*n, m*) "helical" tubes can be either metallic or semiconducting. Though promising advances have been reported[3,4] recently, the most trivial quality issue concerning SWNTs is the lack of the possibility to prepare monodisperse (*n, m*) samples. Moreover, nanotubes tend to form bundles in which several tubes are held together by van der Waals bonding. This bundling may play an important role in future SWNT applications.

Nearly all SWNT purification schemes rely on an oxidative step to clear the nanotubes from amorphous carbon and leftover catalyst particles. However, oxidation itself may change the nanotubes considerably. Albeit Nagasawa et al.[5] report SWNTs to be relatively inert to oxidation using acids, some other groups have found it possible to generate carboxyl groups on nanotubes by treatment in HNO_3[6] or in H_2O_2/H_2SO_4.[7] The presence of carboxyl groups was proven by IR[8] and ^{13}C NMR[9] spectroscopy. The amount of defect sites possibly serving as carboxyl group anchors was estimated to be 6% end-group/1.5% SWNT wall and 5% SWNT wall by this NMR and a thermal decarboxylation study,[10] respectively. Indeed, oxidation by nitric acid is now agreed to be the simplest SWNT modification way, serving as a basis for more advanced functionalization.[8]

All this evidence makes it imperative to examine the relationship between SWNT oxidation and bundle formation. The question was first addressed by Shelimov et al.,[11] who on the basis of TEM images reported that bundles in a raw SWNT material are significantly thinner then those found in a sonicated and HNO_3-oxidized sample. They attributed this phenomenon to a change in sample morphology from a random SWNT mat into spontaneously aligned nanotube "superropes". Another explanation for the apparent bundle thickening was offered by Bower et al.,[12] who used XRD evidence to suggest that HNO_3 molecules are intercalated into the bundle lattice. In this contribution, we present a detailed Raman analysis of the stacking behavior of oxidatively functionalized SWNTs. Our approach is based on the evaluation of the upshift of the first spectral moment of the Raman radial breathing mode (RBM), which has recently been demonstrated[13] to depend selectively

* E-mail: akos@ap.univie.ac.at. Tel: +43 1 4277 51369. Fax: +43 1 4277 51375.
† Universität Wien.
‡ Universität Erlangen.
§ TU Wien.

10.1021/jp014019f CCC: $22.00
Published on Web 06/04/2002

on the number of tubes in the bundle and can thus be used to determine the latter.[14]

Experimental Section

The starting SWNT material was prepared by a modified arc discharge process.[15] The resulting nanotubes were cleaned from the other reaction products by solubilization in aqueous sodium dodecylsulfate (SDS) solution followed by centrifugation and 2×1 min of treatment with an ultrasonic tip (60 W). The supernatant liquid was finally decanted and filtered to obtain the pristine SWNT, referred to as sample "PRST" from now on. The oxidized nanotubes were prepared from the PRST sample following the procedure described previously by Holzinger et al.[16] Samples treated with 14.3 M (3 h) and 2.6 M HNO_3 (11 h) will be labeled "14MOX" and "2MOX", respectively. A portion of the 14MOX sample was annealed in a vacuum better than 1.5×10^{-3} Pa at 1073 K for 12 h to produce the sample "14MOXHT".

Optical transmission was studied for thin sample films on quartz with a Hitachi U-3410 spectrometer in the spectral range between 0.5 and 3.5 eV with a spectral resolution of 20 meV. Infrared spectra were recorded from 1024 scans in vacuum in a reflection−absorption geometry arrangement built into a Bruker FTS66v spectrometer operating in the spectral range 6000−400 cm^{-1} with a spectral resolution of 0.5 cm^{-1}. Raman spectra were recorded in the spectral windows of the RBM and G line with six different lasers extending from 457 to 647 nm (1.92−2.71 eV) with a spectral resolution of 2 cm^{-1}. Analysis and detection of the scattered light was performed with a Dilor xy spectrometer and a liquid N_2 cooled CCD detector. SEM was performed using a Philips XL-40 instrument with a heated LaB_6 cathode. All experiments were performed at room temperature.

Samples for the spectroscopic measurements were prepared by first suspending the SWNT samples in tetrahydofuran (THF) and then drop-coating them on either a hot thin quartz disk (for the UV−vis−NIR experiments) or a hot gold mirror cast on a clean silicon wafer (for the IR and Raman experiments). The solvatation behavior of our four samples was considerably different. While it took only 5 min to prepare the thick gray THF suspension of the pristine sample, 2 h were necessary to reach the same state with the 14MOX sample, and samples 14MOXHT and 2MOX were even harder to the suspend. Prior to the measurements, the samples were heated to 500 K for 12 h in a vacuum better than 5×10^{-3} Pa to remove traces of leftover solvent and adsorbed contaminants. SEM was performed on bulk samples mounted on Al sample holders covered with conducting glue.

Results

The IR spectrum of the oxidized samples is compared with those of PRST and 14MOXHT in Figure 1. Bands induced by the oxidation process are clearly visible at 1580 and 1730 cm^{-1}. A very similar peak structure has been reported by Chen et al.[8] for oxidized SWNTs and was assigned to the presence of carboxyl groups. The 1580 cm^{-1} band has a shoulder at 1530 cm^{-1}. Since this is present in PRST as well, it is not thought to be related to the HNO_3 treatment. The occurrence of carboxyls was confirmed in our samples by the recent ^{13}C NMR studies of Bac et al.,[9] who estimated the amount of functionalized carbon atoms residing in the SWNT wall to be 1.5%. It was possible to partly reproduce the original IR spectrum of the PRST material by annealing the oxidized samples. The relative intensity of the 1530 cm^{-1} band increased during this process.

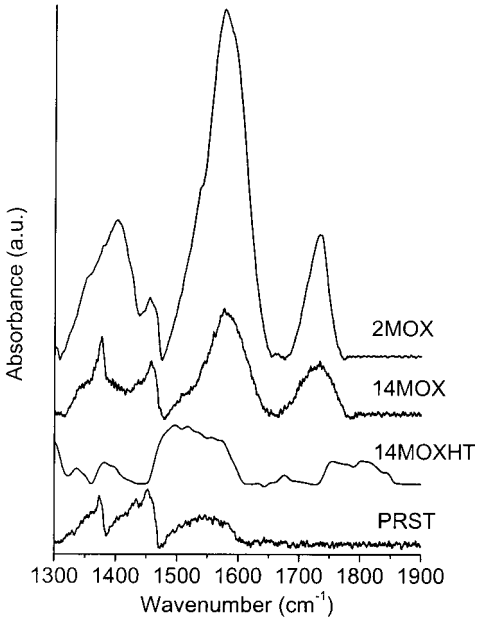

Figure 1. MIR spectra of pristine (PRST), functionalized (14MOX and 2MOX), and annealed (14MOXHT) SWNTs after baseline subtraction and normalizing all spectra to the intensity of the 1455 cm^{-1} peak.

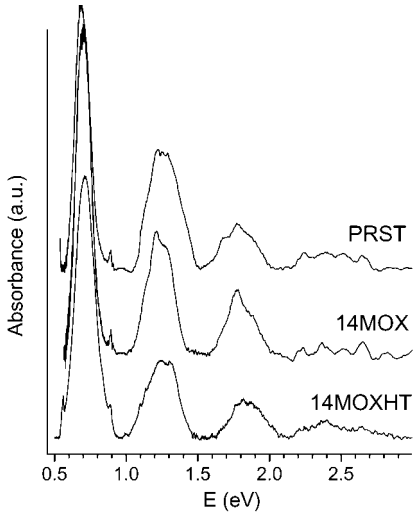

Figure 2. Optical absorption spectra of pristine (PRST), oxidized (14MOX), and annealed (14MOXHT) SWNTs after baseline subtraction.

Optical absorption spectra obtained after subtracting the overall background are presented in Figure 2. for the PRST, 14MOX, and 14MOXHT samples. Absorption peaks are clearly observed in all samples for the first, second, and even for the third transitions between DOS singularities for semiconducting tubes (at 0.7, 1.2, and ~2.5 eV) and for the first transition in metallic tubes (at 1.8 eV). The widths of the transitions increase with increasing energy from about 150 to 800 meV. This broadening is a consequence of a rather broad diameter distribution in the tube material. On the other hand, the well-expressed peaks observed even for the functionalized tubes indicate that the samples were able to maintain their one-dimensional electron structure during oxidation and annealing. For the functionalized tubes, the transitions for the metallic and the third transition for the semiconducting tubes are slightly upshifted by about 100 meV and broadened. This upshift is not recovered by the annealing process. Numerous weak peaks between 2.2 and 2.8 eV arise from the clustering of diameters in the distribution.[14]

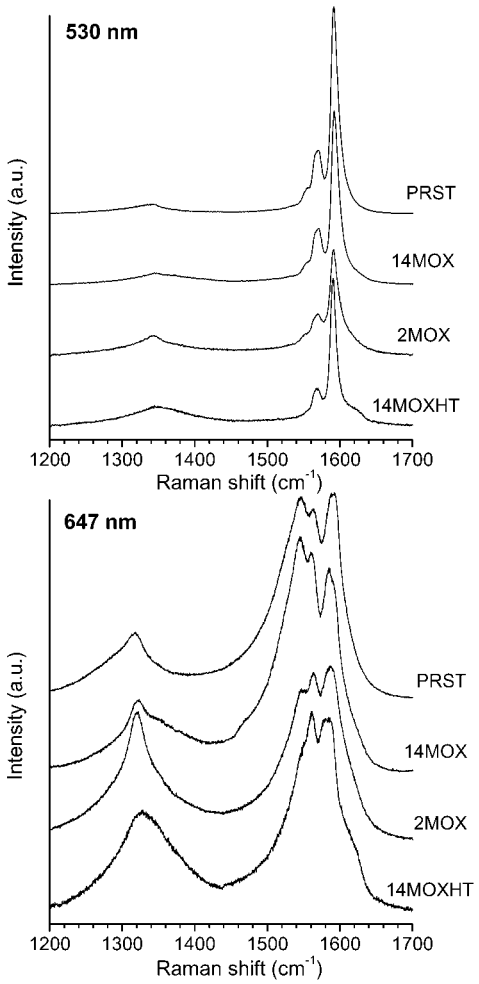

Figure 3. D line and G line region of the Raman spectra of the samples at two selected laser wavelengths after subtracting a constant background. The 530 nm laser probes primarily semiconducting while the 647 nm laser probes metallic SWNTs.

The Raman spectrum of SWNTs has three important regions. The first one around 1580 cm^{-1} is strongly related to the tangential Raman mode in graphite and is referred to as the "G line". The G line is known to consist of several components. For red laser excitation, the peak response is shifted to about 1550 cm^{-1} and the low-frequency part of the line exhibits a Fano character. The structure around 1340 cm^{-1} is called the "D line" and is related to scattering from defects present in the SWNT sample. The third region between 140 and 220 cm^{-1} originates from a radial breathing mode (RBM) and is unique for SWNTs. In Figure 3. we present the D and G line spectral region of the samples at two selected laser wavelengths. Spectra recorded at other laser energies (457, 496, 514, and 568 nm) were rather similar to the one measured at 530 nm, since these lasers all probe semiconducting tubes.[17]

As expected, the spectrum measured with a 647 nm laser is different from the others because in this case the C−C stretching modes of metallic SWNTs are brought into resonance.[18] The rather high value of 1:10 for the integrated intensity ratio between the D line and the G line observed even for the pristine material indicates a high defect concentration. After functionalization, this value increased yet to about 1:4. The metallic character expressed by the low-energy wing of the G-line pattern remains fairly unchanged.

No peak shift is observable for the G line for any of the samples. In contrast to this, the D-line is upshifted upon

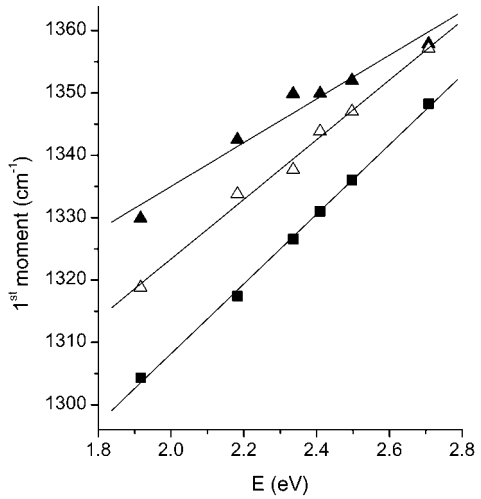

Figure 4. Line position of the first moment of the D line in pristine and functionalized SWNT as a function of excitation energy. Full squares, pristine material (PRST); full triangles, functionalized with 14M HNO_3 (14MOX); and open triangles, annealed after functionalization (14MOXHT).

chemical treatment, as explicitly demonstrated in Figure 4 for excitation with various lasers. Not only the absolute value of the peak position is enhanced but also the slope of the dispersion changes from the 55.9 ± 1.2 cm^{-1}/eV value of the PRST sample to the 35.1 ± 3.7 cm^{-1}/eV value of the 14MOX sample. After heat treatment, the original behavior is only partly recovered, as indicated by the intermediate slope of 47.8 ± 2.2 cm^{-1}/eV.

In Figure 5, the RBM spectral window is presented for all six laser energies. It can be observed here that

(i) the RBM produces the well-known fine structure which changes with laser energy[19] and which is caused by a diameter-selective Raman scattering process and a clustering of the diameters in the distribution,[14] and

(ii) the RBM of the oxidized samples is clearly upshifted compared to that of pristine sample while the overall line shape remains similar. The differences between the line shape of pristine and oxidized tubes increase while shifting from deep blue to red lasers. This is a consequence of the higher sensitivity or the response to differences in the optical properties at low laser energies.[14] The value of the upshift does not change with the laser energy and is about 9 cm^{-1}.

Discussion

While the 1730 cm^{-1} band in the IR spectrum of the functionalized samples presented in Figure 1 can be clearly assigned to ν(C═O) vibrations of −COOH groups attached to the nanotube surface,[8] the origin of the 1580 cm^{-1} band is not clear yet. We may tentatively assign it to carboxyl groups attached to electron-rich defects. However, it may also indicate the presence of carboxyl dimers, since H-bonding is known[20] to lower the frequency of the C═O stretching vibration considerably. The intensity of the 1730 and 1580 cm^{-1} bands decreased significantly upon annealing at 1073 K, thus providing further evidence that both originate from vibrations related to the carboxyl groups which are removed during the thermal decarboxylation. The relative intensity of the 1530 cm^{-1} shoulder is larger in 14MOXHT than in the oxidized samples; therefore, it is probably not related to the HNO_3 generated carboxyl groups. Since the band is observable in PRST as well, it could be related to some amorphous carbon species contaminating the samples. A more detailed analysis, based on the expectation that the amount of such amorphous carbon should

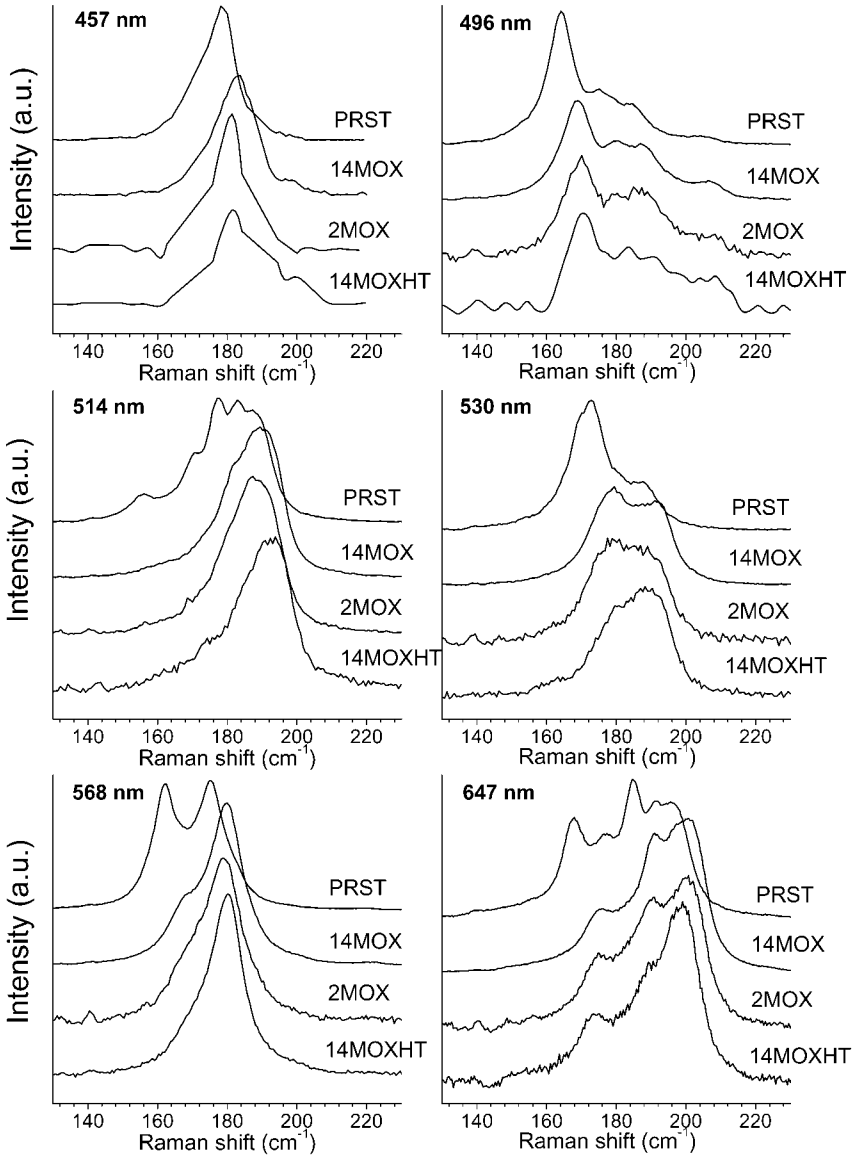

Figure 5. Radial breathing mode (RBM) Raman response of pristine and functionalized SWNT as excited with six different laser lines.

increase with functionalization-annealing cycles, is required for the unambiguous assignation of this band.

It is noteworthy in the optical absorption spectra (Figure 2.) that the fine structure of the 1.2 and 1.8 eV peaks in the 14MOX spectrum is different from that of the PRST material, but becomes similar to the PRST again after annealing (14MOXHT spectrum). This latter fact is in agreement with the IR results and is readily explained by the small distortions introduced into the SWNT electron system when forcing certain carbon atoms into an sp^3 state by oxidation. A fraction of these atoms changes back to sp^2 during thermal decarboxylation, and thus, a spectrum resembling the original PRST is obtained. The 100 meV upshift of the 1.8 and 2.5 eV peaks is probably related changes in the DOS due to some holes etched into the sidewalls of the tubes which cannot be annealed away by the heat treatment. These defect sites may also be responsible for the increase of the intensity of the 1530 cm^{-1} band in the IR spectrum. According to Jost et al.,[21] the absence of major peak shifts in the optical absorption spectrum suggests that the characteristic distribution of SWNT diameters remained the same throughout the experiments.

A plausible explanation for the changes in the Raman resonance behavior would be the doping of the SWNTs by nitric acid molecules or NO_x residues. Indeed, HNO_3 intercalation has already been suggested to occur in SWNTs by Bower et al.[12] However, molecules intercalated into a SWNT bundle are expected to act as doping agents, and SWNT bundles have been shown[22] to exhibit considerable upshifts or downshifts in the main component of the G line upon p- and n-type doping, respectively. Albeit no such shifts are visible in Figure 3, we have performed spectral decomposition on the G line of two selected samples. The G line of the pristine tubes as measured with the 530 nm laser could be fitted by five Lorentzian curves. For the functionalized tubes, one additional line at 1615 cm^{-1} was required for the fit. Since this line is retained after heating, it is assigned to defects in the wall of the tubes. While it was also possible to fit the G line measured at 647 nm with Lorentzians (seven Lorentzians are needed), we have found that a better fit quality can be achieved using one Fano type and three Lorentzian curves. Again for the functionalized tubes, an additional line at 1615 cm^{-1} was required. Results of the fits are presented in Figure 6, and parameters of the curves are given in Table 1. It is clearly seen from the data that there is a small broadening of the spectral components of the G-line, but the changes in their positions are well within experimental error and cannot be interpreted as a doping-induced shift. The lack

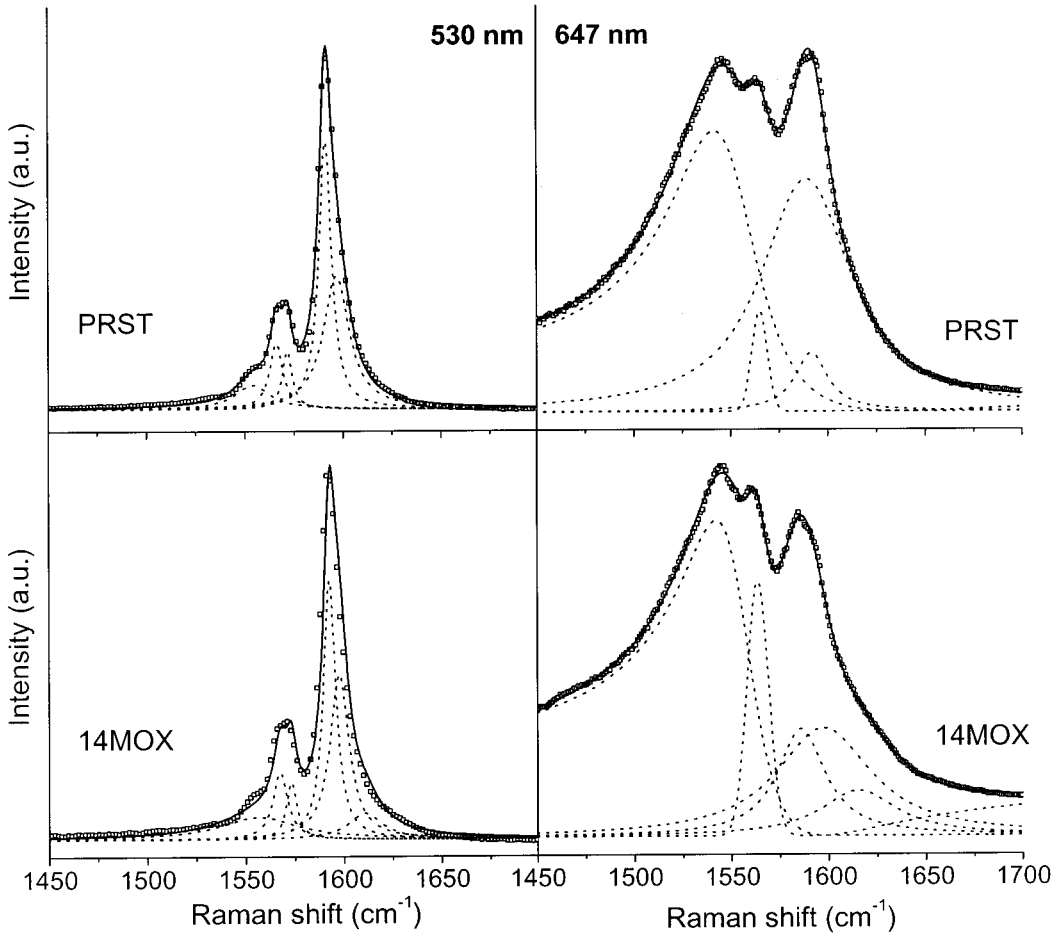

Figure 6. Reproducing the G line region of two selected samples (PRST and 14MOX) for two selected laser wavelengths at 530 and 647 nm as a superposition of Lorentzian curves and as a superposition of Lorentzian curves and a Fano line, respectively. Hollow squares mark experimental data, dotted lines denote the individual peak functions, and a solid line represents the envelope of the fitted peaks.

TABLE 1: Frequencies[a] (ϖ) and Full-width at Half Maximum Intensity[a] (γ) of the Curves Used To Fit the Bands Forming the G Line in the Raman Spectrum of SWNTs

	530 nm				647 nm			
	PRST		14MOX		PRST		14MOX	
line	ϖ	γ	ϖ	γ	ϖ	γ	ϖ	γ
Fano					1542	68	1542	74
Lorentz 1	1554	21	1556	48	1565	11	1564	16
Lorentz 2	1566	8	1566	9	1589	56	1586	25
Lorentz 3	1572	6	1572	6	1591	17	1597	58
Lorentz 4	1591	8	1591	8			1615	47
Lorentz 5	1597	16	1596	12				
Lorentz 6			1610	21				

[a] In inverse centimeters.

of significant changes in the shape and in the parameters of the Fano line is again consistent with the conservation of the metallic character of the tubes after functionalization.

The first moments (center of gravity) of the spectral pattern for the RBM were shown recently to exhibit an oscillatory behavior if plotted versus the energy of the exciting laser.[14] Any change in intertube coupling shifts this oscillations to higher or lower frequencies without any phase shift. In contrast, any change in tube diameter distribution shifts the oscillation and contributes to the phase. The evaluated first and second moments of the spectra presented in Figure 5 are therefore plotted in Figure 7 and marked by individual symbols. The phase of the first moment's oscillation is not affected by the oxidation. This

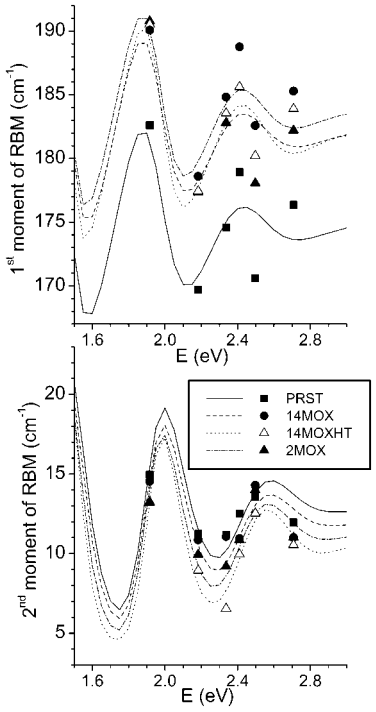

Figure 7. Fitting of the spectral moments of the Raman radial breathing mode using the continuum approximation. The two graphs share the same legend; individual symbols represent experimental data while curves are calculated from the fits.

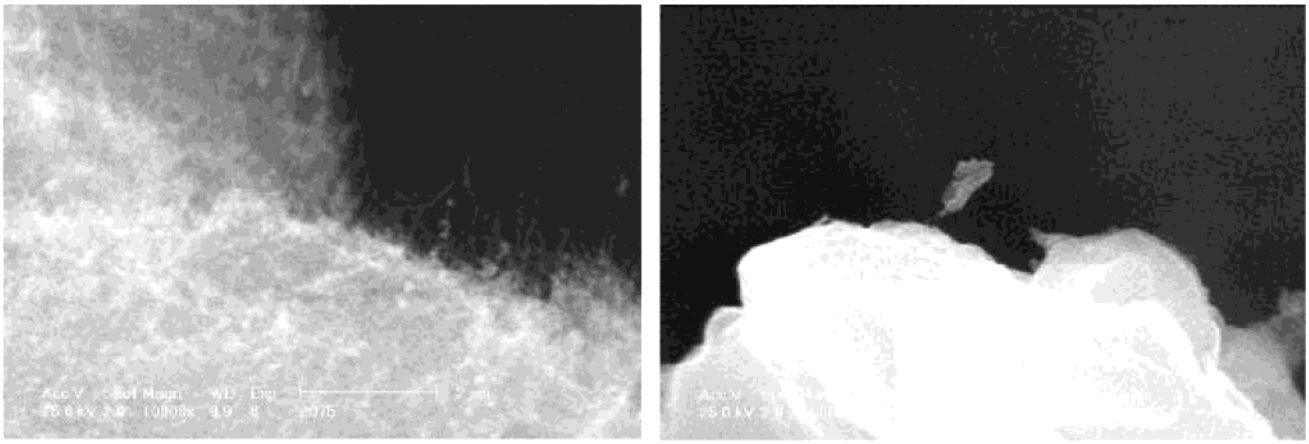

A B

Figure 8. Typical SEM images of pristine (A) and oxidized (B) SWNTs. The change from the loose random to the dense layered texture is attributed to the alignment of thickened nanotube bundles.

TABLE 2: Calculated Parameters of the SWNT Samples Studied Here[a]

	d (nm)	σ (nm)	C_2 (cm^{-1})	N	d_{bundle} (nm)
PRST	1.44	0.13	9.2	5	4.7
14MOX	1.45	0.13	14.3	34	12.5
14MOXHT	1.45	0.11	14.5	38	13.3
2MOX	1.45	0.12	15.7	98	21.4

[a] Key: d is the average diameter of an individual tube, σ is the width of the diameter distribution (equivalent to the fwhm of the corresponding Gaussian), C_2 is the intertube interaction constant, N is the number of tubes per bundle as calculated from C_2, and d_{bundle} is the bundle diameter as calculated from d and N.

again confutes the assumption that the RBM upshift is caused by changes in the SWNT diameter distribution.

Furthermore, the idea of an oxidation-induced RBM upshift contradicts common chemical intuition as well. Since the frequency of the RBM mode scales with $1/d$, an upshifted RBM should be interpreted as a loss of large diameter tubes accompanied by a relative gain in small diameter SWNTs. However, the pyramidalization angle and, consequently, the expected chemical reactivity of thin tubes is larger than that of the thicker ones. Therefore, if the position of the RBM would vary at all because of SWNT diameter distribution changes related to chemical reactions, the alteration would be much more likely a downshift than an upshift.

Having ruled out two possible explanations for the RBM upshift which would call for a different theoretical approach, we can now apply a quantitative fit procedure on the spectral moments to yield the average tube diameter (d), the width of diameter distribution (σ), and an intertube interaction constant C_2. The reader is referred to Kuzmany et al.[14] for the details of the calculation. It is enough to note here that our target function in the fit procedure was calculated within the so-called "continuum approximation", which substitutes the explicit DOS function for each tube by a constant value supplemented by δ-functions for the van Hove singularities and considers only the first few (in our case, eight) transitions between the latter in the DOS. Results of the fitting are presented in columns 1−3 of Table 2. As expected, the center and the width of the SWNT diameter distribution do not change upon nitric acid treatment. However, the value of the intertube interaction constant C_2 increases significantly.

A quantitative relationship between the values obtained for d and C_2 and the average number of SWNTs in a bundle has been recently suggested by Henrard et al.[13] By application of this equation, the N values in column 4 of Table 2 were derived, and from d and N, the bundle diameter d_{bundle} (column 5, Table 2) was calculated assuming a triangular SWNT lattice. It should be noted that in this model the upshift of the RBM with the bundle diameter saturates somewhere above $N = 100$, the exact value depending on the individual sample, and therefore, values for N obtained this way could be subjects to considerable error. On the other hand, the N values are believed to be comparable by "smaller−larger" type of judgement even if they are not absolutely correct.

The results of Table 2 are consistent with the difference in the solvatation behavior of the samples as it was described above. The following interpretation can be offered. Thinner nanoropes are obviously easier to suspend than thicker ones because of their smaller mass and larger surface-to-bulk ratio. Considering the significant differences between the average number of tubes forming the bundles in the PRST, 14MOX, and 2MOX samples (5, 34, and 98, respectively), the decreasing trend in suspendability is ready explained. The difference between samples 14MOX and 14MOXHT might be assigned to the thermal decarboxylation of the latter. It is rather possible that a lightly polar solvent like THF solvates a SWNT sample with −COOH groups on its walls better then one of the same bundle size, but deprived of its polar sidegroups.

The final conclusion from Table 2 is that SWNT bundles get thicker during HNO_3 treatment performed as described above and do not get thin again during thermal annealing. The interpretation given for the Raman data is supported by the following facts:

(i) it offers an explanation for the in-phase upshift of the Raman RBM of SWNTs upon oxidation,

(ii) it explains the differences observed in the solvatation properties of the samples, and

(iii) it is in agreement with the previous TEM observations of Shelimov et al.[11] On the other hand, we cannot completely exclude the possibility that the upshift of the RBM originates from a different phenomenon.

A feasible interpretation for the bundle thickening would be that several randomly oriented SWNTs from the pristine sample align parallel during oxidation. The major driving force of this process would certainly be the van der Waals interaction[23] between tubes. However, on the basis of our results, we are tempted to suggest that H-bonding between carboxyl groups

attached to the walls of functionalized SWNTs also add to the overall stacking effect. Observations supporting this assumption are the following: (i) the appearance of the 1580 cm^{-1} peak in the IR spectra of the functionalized material, which might be related to −COOH dimers, and (ii) the correlation between the larger number (assumed on the basis of more intense IR ν(C═O) peaks) of carboxyl groups attached to the walls of 2MOX and the larger value of SWNTs per bundle calculated for the 2MOX, as compared to 14MOX.

Direct evidence of the functionalization-induced morphological changes was obtained by SEM and is presented in Figure 8, where parts A and B shown typical images of samples PRST and 2MOX, respectively. The structure of the former appears to be loose and wool-like, dominated by randomly oriented thin entities (SWNT bundles and ropes), while 2MOX is dense and consists of well-defined layers. We suggest that this laminated structure is the result of the spontaneous alignment of the thick nanotube bundles, promoted by the H-bonding between the −COOH sidegroups formed upon oxidation. The striking difference between the detached PRST and the thick 2MOX texture is in agreement with the perceived difference in the solubility of the samples as well.

Summary

IR and optical absorption spectroscopy were utilized to study the formation of carboxyl groups on SWNT walls by oxidation with HNO_3. The carboxyl groups could be removed by thermal decarboxylation without damaging the one-dimensional electron system of the nanotubes, but defects remain on the chain which could be holes in the walls of the tubes. When comparing the Raman radial breathing mode (RBM) region of pristine and oxidized samples, we noticed an intriguing in-phase upshift of the first spectral moment of the RBM upon oxidation. After experimentally ruling out two possible causes for this shift, we suggested that it could be explained by SWNT bundle thickening. The number of tubes per bundle was approximately calculated from the Raman data, revealing a 3−5-fold increase of bundle diameters as compared to those in the pristine material. This is in good agreement with earlier TEM data and can be used to explain the observed differences in the suspendability of SWNTs in THF, as well as the morphological changes found by SEM investigation. We conclude that oxidative functionalization and bundle thickening should be taken into account in studies involving extended contact between SWNTs and nitric acid.

Acknowledgment. We thank Dr. T. Pichler, Mag. R. Pfeiffer, and Mag. W. Plank for experimental assistance. This work was financed through the EU RTN FUNCARS (HPRN-CT-1999-00011) and FWF Austria No. 14893.

References and Notes

(1) Iijima, S.; Ichihashi, T. *Nature (London)* **1993**, *363*, 603.
(2) Ando, Y.; Zhao, X.; Hirahara, K.; Suenaga, K.; Bandow, S.; Iijima, S. *Chem. Phys. Lett.* **2000**, *323*, 580.
(3) Tang, Z. K.; Sun, H. D.; Wang, J.; Chen, J.; Li, G. *Appl. Phys. Lett.* **1998**, *73*, 2287.
(4) Terranova, M. L.; Piccirillo, S.; Sessa, V.; Sbornicchia, P.; Rossi, M.; Botti, S.; Manno, D. *Chem. Phys. Lett.* **2000**, *327*, 284.
(5) Nagasawa, S.; Yudasaka, M.; Hirahara, K.; Ichihashi, T.; Iijima, S. *Chem. Phys. Lett.* **2001**, *328*, 380.
(6) Chiang, I. W.; Brinson, B. E.; Smalley, R. E.; Margrave, J. L.; Hauge, R. H. *J. Phys. Chem. B* **2001**, *105*, 1157.
(7) Yu, Z.; Brus, L. E. *J. Phys. Chem. A* **2000**, *104*, 10995.
(8) Chen, J.; Rao, A. M.; Lyuksyutov, S.; Itkis, M. E.; Hamon, M. A.; Hu, H.; Cohn, R. W.; Eklund, P. C.; Colbert, D. T.; Smalley, R. E.; Haddon, R. C. *J. Phys. Chem. B* **2001**, *105*, 2525.
(9) Bac, C. G.; Latil, S.; Jourdain, V.; Aznar, R.; Rachdi, F.; Bernier, P.; Holzinger, M.; Hirsch, A.; Mathis, C.; Petit, P.; Rubio, A. In *Proc. Int. Winterschool on "Electronic Properties of Molecular Nanostructures", Kirchberg, 2001*; Kuzmany H., et al., Eds.; AIP Conference Proceedings, Melville, NY, 2001.
(10) Mawhinney, D. B.; Naumenko, V.; Kuznetsova, A.; Yates, J. T.; Lin, J.; Smalley, R. E. *Chem. Phys. Lett.* **2000**, *324*, 216.
(11) Shelimov, K. B.; Esenaliev, R. O.; Rinzler, A. G.; Huffman, C. B.; Smalley, R. E. *Chem. Phys. Lett.* **1998**, *282*, 429.
(12) Bower, C.; Kleinhammes, A.; Wu, Y.; Zhou, O. *Chem. Phys. Lett*. **1998**, *288*, 481.
(13) Henrard, L.; Lambin, Ph.; Rubio, A. In *Proc. Int. Winterschool on "Electronic Properties of Molecular Nanostructures", Kirchberg, 2000*; Kuzmany, H., et al., Eds.; AIP Conference Proceedings; Melville, NY, 2000; Vol. 544.
(14) Kuzmany, H.; Plank, W.; Hulman, M.; Kramberger, Ch.; Grüneis, A.; Pichler, Th.; Peterlik, H.; Kataura, H.; Achiba, Y. *Eur. Phys. J. B* **2001**, *22*, 307.
(15) Journet, C.; Bernier, P. *Appl. Phys. A* **1998**, *67*, 1.
(16) Holzinger, M.; Hirsch, A.; Bernier, P.; Duesberg, G. S.; Burghard, M. *Appl. Phys. A* **2000**, *70*, 599.
(17) Pimenta, M. A.; Marucci, A.; Brown, S. D. M.; Matthews, M. J.; Rao, A. M.; Eklund, P. C.; Smalley, R. E.; Dresselhaus, G.; Dresselhaus, M. S. *J. Mater. Res.* **1998**, *13*, 2396.
(18) Pimenta, M. A.; Marucci, A.; Empedocles, S. A.; Bawendi, M. G.; Hanlon, E. B.; Rao, A. M.; Eklund, P. C.; Smalley, R. E.; Dresselhaus, G.; Dresselhaus, M. S. *Phys. Rev. B* **1998**, *58*, R16016.
(19) Rao, A. M.; Richter, E.; Bandow, S.; Chase, B.; Eklund, P. C.; Williams, K. W.; Menon, M.; Subbaswamy, K. R.; Thess, A.; Smalley, R. E.; Dresselhaus, G.; Dresselhaus, M. S. *Science* **1997**, *275*, 187.
(20) Schrader, B., Ed. *Infrared and Raman Spectroscopy;* VCH: Weinheim, 1995; Chapter 4.
(21) Jost, O.; Gorbunov, A. A.; Pompe, W.; Pichler, T.; Friedlein, R.; Knupfer, M.; Reibold, M.; Bauer, H.-D.; Dunsch, L.; Golden, M. L.; Fink, J. *Appl. Phys. Lett.* **1999**, *75*, 2217.
(22) Rao, A. M.; Bandow, S.; Richter, E.; Eklund, P. C. *Thin Sol. Films* **1998**, *331*, 141.
(23) Thomsen, C.; Reich, S.; Goñi, A. R.; Jantoljak, H.; Rafailov, P. M.; Loa, I.; Syassen, K.; Journet, C.; Bernier, P. *Phys. Stat. Sol. (B)* **1999**, *215*, 435.